ACSNANO

www.acsnano.org

ARTICLE

Nano Secondary Ion Mass Spectrometry Imaging of Dopamine Distribution Across Nanometer Vesicles

Jelena Lovrić,[†,‡] Johan Dunevall,[†] Anna Larsson,[§] Lin Ren,[†] Shalini Andersson,[∥] Anders Meibom,[⊥] Per Malmberg,[†,‡] Michael E. Kurczy,[∥] and Andrew G. Ewing*[,†,‡,§]

[†]Department of Chemistry and Chemical Engineering, Chalmers University of Technology, Gothenburg SE-412 96, Sweden

[‡]National Centre for Imaging Mass Spectrometry, Chalmers University of Technology and University of Gothenburg, Gothenburg SE-412 96, Sweden

[§]Department of Chemistry and Molecular Biology, University of Gothenburg, Gothenburg SE-412 96, Sweden

[∥]Cardiovascular and Metabolic Diseases, Innovative Medicines and Early Development Biotech Unit, AstraZeneca, Mölndal SE-431 50, Sweden

[⊥]Laboratory for Biological Geochemistry, École Polytechnique Fédérale de Lausanne and Center for Advanced Surface Analysis, Institute of Earth Sciences, University of Lausanne, Lausanne CH-1015, Switzerland

Supporting Information

ABSTRACT: We report an approach to spatially resolve the content across nanometer neuroendocrine vesicles in nerve-like cells by correlating super high-resolution mass spectrometry imaging, NanoSIMS, with transmission electron microscopy (TEM). Furthermore, intracellular electrochemical cytometry at nanotip electrodes is used to count the number of molecules in individual vesicles to compare to imaged amounts in vesicles. Correlation between the NanoSIMS and TEM provides nanometer resolution of the inner structure of these organelles. Moreover, correlation with electrochemical methods provides a means to quantify and relate vesicle neurotransmitter content and release, which is used to explain the slow transfer of dopamine between vesicular compartments. These nanoanalytical tools reveal that dopamine loading/unloading between vesicular compartments, dense core and halo solution, is a kinetically limited process. The combination of NanoSIMS and TEM has been used to show the distribution profile of newly synthesized dopamine across individual vesicles. Our findings suggest that the vesicle inner morphology might regulate the neurotransmitter release event during open and closed exocytosis from dense core vesicles with hours of equilibrium needed to move significant amounts of catecholamine from the protein dense core despite its nanometer size.

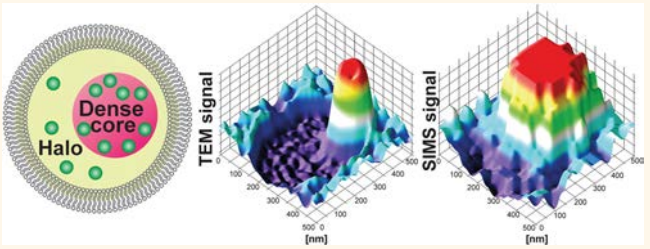

KEYWORDS: *nanoimaging, NanoSIMS, vesicle content, electrochemistry, nanocompartments*

Chemical communication in eukaryotic cells relies heavily on loading and trafficking of secretory vesicles to the plasma membrane. Upon stimulation, the loaded, docked secretory vesicles fuse with the plasma membrane and discharge their neurotransmitter cargo into the extracellular space. This process, called exocytosis, is fundamental and highly regulated.[1,2] Regulation of exocytosis has been widely studied, and the understanding of its mechanism is still under debate. Several mechanisms have been reported such as all-or-nothing release during which vesicles completely fuse with the plasma membrane and release their total content.[3] Contrary to the all-or-nothing mode, partial release mechanisms have been proposed, suggesting the transient opening of the fusion pore between the cell membrane and secretory vesicle followed by closing again.[4] In addition to the release event, exocytosis is also regulated through vesicle loading. In general, this process involves a neurotransmitter transporter, an integral vesicle membrane protein that uses the pH gradient across the vesicle membrane, to drive uptake of neurotransmitters into the vesicle.[5−8] Defining the vesicle storage mechanisms would be an important piece of the exocytosis regulation puzzle.[5,9,10]

Several cell types have been employed for loading studies among which neuroendocrine cells have had an important role

Received: October 26, 2016
Accepted: December 20, 2016
Published: December 20, 2016

DOI: 10.1021/acsnano.6b07233
ACS Nano XXXX, XXX, XXX−XXX

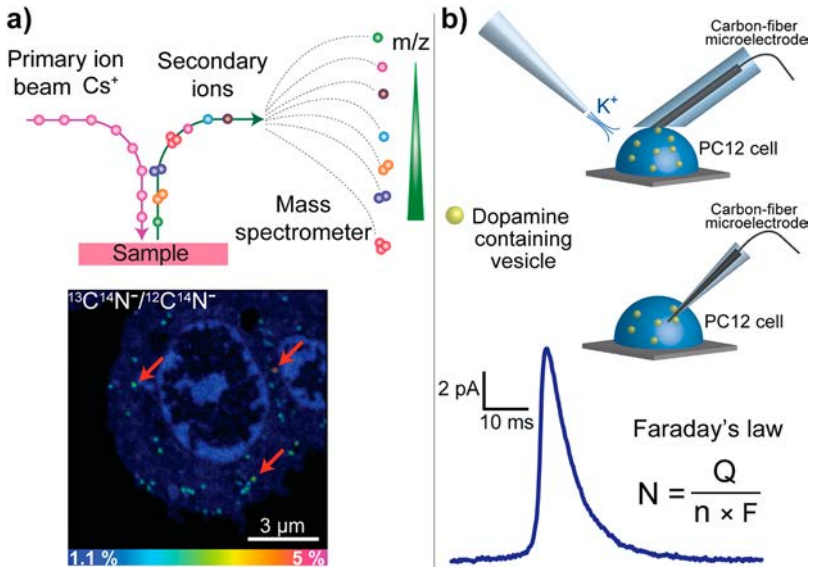

Figure 1. NanoSIMS and its correlation to amperometric techniques. (a) NanoSIMS. Top: principle of NanoSIMS analysis. Bottom: $^{13}C^{14}N^-/^{12}C^{14}N^-$ ratio image reveals the dopamine enrichment in single vesicles. We highlight three examples of vesicles in the NanoSIMS image with red arrows. (b) Amperometric techniques. Top: Single cell amperometry principle. Middle: Intracellular vesicle electrochemical cytometry principle. Bottom: Amperometric current transients allow, by applying Faraday's law, calculation of the mole amount of dopamine that is oxidized from each exocytotic release or individual vesicle (N). Q is the charge calculated from the time integral of current peak from the amperometric trace, n is the number of electrons exchanged in the oxidation reaction ($2e^-$ for dopamine), and F is the Faraday constant (96,485 C mol^{-1}).

as a model system. They possess two types of secretory vesicles, synaptic-like microvesicles (SLMVs) and so-called large dense-core vesicles (LDCVs). The larger LDCVs typically have diameters around 150−300 nm and an inner morphology due to the presence of a protein core surrounded with a lucent solution, typically called the halo.[6,11,12] Neuroendocrine LDCVs are rich in catecholamine neurotransmitters. These chemicals are introduced into the vesicle interior *via* the vesicular monoamine transporter 1 (VMAT1), one of two identified isoforms of VMAT which show substantial differences in their physiology and pharmacology.[8] The rat endocrine cell line, pheochromocytoma (PC12), is a type of neuroendocrine cell that is a robust model to study the mechanism of vesicle storage and pharmacology. This cell line exhibits a number of important neuronal properties[13,14] and shows preferential expression of VMAT1 on LDCVs which recognizes dopamine and norepinephrine present in these cells.[6]

Pharmacological modulation of VMAT1 activity has been observed with amperometry techniques, and sustained transporter activity was reported to be important for maintaining vesicle content.[12,15,16] Indeed, with its high temporal resolution capability and possibility to quantify the content of electroactive neurotransmitters, amperometry has been a widely used electrochemical technique in the quest of understanding the role of VMAT in vesicle transmitter storage. This electrochemical approach revealed that treatment with the catecholamine metabolic precursor, L-3,4-dihydroxyphenylalanine (L-DOPA), increases the dopamine transmitter quantal size.[10,12,15−17] In contrast to L-DOPA, the drug reserpine removes dopamine from vesicles. A reserpine-L-DOPA dichotomy has been observed with transmission electron microscopy (TEM) as vesicle shrinking or swelling, following reserpine or L-DOPA treatment, respectively.[12] However, this technique does not provide chemical information.

Advances in secondary ion mass spectrometry (SIMS) imaging, such as improvements in detection limit and spatial resolution, have made the SIMS analytical techniques applicable for chemical imaging in biological research. One such technique, nanoscale SIMS (NanoSIMS) provides excellent mass and spatial resolution with low detection limits. NanoSIMS has traditionally been used to analyze inorganic materials collecting either positively or negatively charged species.[18] In biological research, negative species are typically monitored. The basic operation of NanoSIMS in negative mode involves a high-energy Cs^+ primary ion beam that scans the sample surface and sputters away secondary particles. The secondary ions are analyzed with a dual-focusing sector mass analyzer and separated based on their mass to charge ratio (m/z). Due to the high rate of sample fragmentation, detection is generally limited to monatomic and diatomic secondary ions. These small ions are ubiquitous, thus to gain chemical information, the molecules of interest are usually isotopically labeled.[19,20] The outstanding spatial resolution of NanoSIMS allows tracking the labeled molecules within single cells.[21,22]

In this paper, we image the dopamine content inside single nanometer LDCVs in PC12 cells with NanoSIMS. In order to image vesicle transmitter content, cells were treated with ^{13}C-labeled L-DOPA, a metabolic precursor of dopamine. By correlating TEM to NanoSIMS images of a single vesicle, we distinguish the distribution of isotopically labeled dopamine across the vesicle interior and in subvesicular compartments. Correlation between imaging and electrochemical data allowed us to count the numbers of molecules in the vesicles, as well as those released in exocytosis, and compare this to the relative quantification of the NanoSIMS. We show that loading and unloading of the vesicular dense core is a kinetically limited process, reflecting both loading of messengers and release into and out of the nanometer protein dense core with a time scale on the order of hours.

DOI: 10.1021/acsnano.6b07233
ACS Nano XXXX, XXX, XXX−XXX

RESULTS AND DISCUSSION

We carried out NanoSIMS (Figure 1a) by imaging pheochromocytoma (PC12) cells loaded with dopamine biosynthesized from ^{13}C-L-DOPA to examine the nanometer environment inside of catecholamine vesicles. Furthermore, to be able to validate results obtained with NanoSIMS imaging, we correlated SIMS imaging data with data collected from amperometry techniques (Figure 1b). The transmitter release upon stimulation was measured with single cell amperometry,[23] whereas dopamine vesicle content was determined with a newly developed technique called intracellular vesicle electrochemical cytometry.[10]

Imaging Chemical Content of Single Vesicles by NanoSIMS. We began by chemically imaging the ^{13}C-dopamine content of LDCVs in PC12 cells. To avoid the obstacles associated with identifying specific sample features during SIMS acquisition, we combined the TEM and NanoSIMS imaging techniques.[24−26] The sample preparation method used in this work is conventional in electron microscopy and also applicable to NanoSIMS imaging. Cells were chemically fixed in order to preserve morphology and capture the intravesicular dopamine. The application of aldehydes during the initial phase preserved dopamine *in situ via* the formation of an imine bond between the primary amine and the aldehyde group of the fixative.[27] Ultrathin cell sections were placed onto TEM grids supported with Formvar and stabilized with evaporated carbon. The Formvar-carbon support was important to maintain sample stability during NanoSIMS analysis.

In order to use NanoSIMS to visualize the loading of ^{13}C-dopamine, we incubated cells with ^{13}C-L-DOPA (Figure 2d). Additionally, this allowed us to investigate the impact of reserpine on the vesicle storage mechanism (Figure 2b, c, and e), which was administered to the cells for 1 h in all experiments. Figure 2 shows three panels of images for five different cell treatments. The left panel shows TEM images of PC12 cells, which confirms that the cell structure was preserved and clearly reveals the localization of the LDVCs. The spatial distribution of the $^{12}C^{14}N^-$ ion (middle panel) discloses the morphological information based on the endogenous chemical signal from all carbon-nitrogen containing ions. The right panel presents hue-saturation-intensity (HSI) images of the quantified $^{13}C^{14}N^-/^{12}C^{14}N^-$ isotopic ratio, revealing local isotopic enrichments of ^{13}C-dopamine on a color scale ranging from dark blue (^{13}C-natural abundance; 1.1% of all carbon present in nature) to red/pink, and directly reflecting the isotopic enrichment. As expected, based on visual inspection, untreated control PC12 cells did not give rise to an isotopic ratio signal, whereas cells treated with ^{13}C-L-DOPA only showed colocalization of dopamine enrichment within LDCVs, which were clearly identified in the TEM image (Figure 2d). This is also shown in an enlarged image of vesicles in Figure S1. Moreover, cells treated with ^{13}C-L-DOPA prior to reserpine showed very little enrichment in ^{13}C-dopamine (Figure 2b). These observations confirm that NanoSIMS has the potential to assess storage dynamics in single vesicles and led to the next step; a detailed analysis of dopamine loading and enrichment in individual vesicles.

Partitioning of Vesicular Dopamine. In order to obtain insights into vesicle loading dynamics, in addition to visual inspection, we compared the mean ^{13}C-dopamine enrichment per vesicle for each treatment group. As the number of vesicles per cell varied, we normalized the mean value of ^{13}C-dopamine enrichment obtained from each PC12 cell of the treatment group with the mean of the vesicle density (number of vesicles per surface area) for the treatment group (Figure 2). In Figure 3a we show a comparison of normalized enrichment for the different treatment groups where ^{13}C-L-DOPA was administrated for 1.5 h before or after the reserpine treatment or alone.

Control cells did not show enrichment in ^{13}C-dopamine, and the highest values were measured in the sample treated with ^{13}C-L-DOPA alone. Reserpine administration after ^{13}C-L-DOPA incubation, the treatment labeled as LD(1.5 h)+R (LD is L-DOPA, S is a short 1.5 h exposure, R is reserpine) depleted

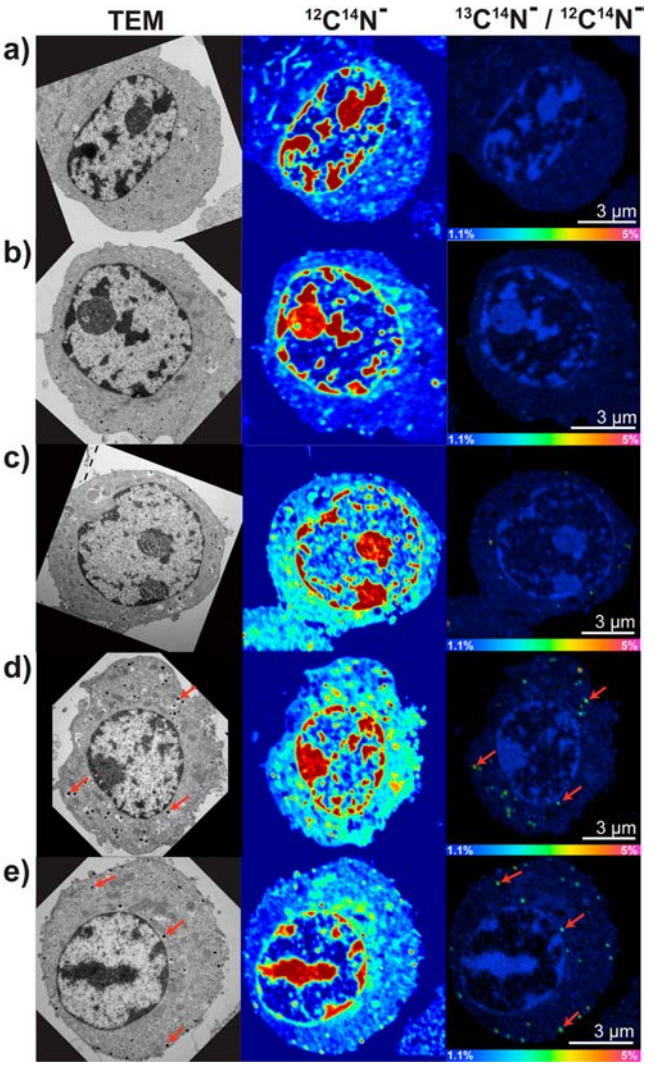

Figure 2. TEM and NanoSIMS images of PC12 cells treated with ^{13}C-L-DOPA and reserpine. From left to right: Corresponding TEM image, NanoSIMS image of $^{12}C^{14}N^-$ ion species, and HSI (hue-saturation-intensity) image of $^{13}C^{14}N^-/^{12}C^{14}N^-$ ratio. (a) Control PC12 cell. Ion images: 8 layers, FoV: 10 × 10 μm. (b) L-DOPA (1.5 h) and reserpine treated PC12 cells. Ion images: 6 layers, FoV: 9 × 9 μm. (c) L-DOPA (12 h) and reserpine treated PC12 cells. Ion images: 8 layers, FoV: 11 × 11 μm. (d) L-DOPA (1.5 h) treated PC12 cells. Ion images: 6 layers, FoV: 11 × 11 μm. (e) Reserpine and L-DOPA (1.5 h) treated PC12 cells. Ion images: 4 layers, FoV: 9 × 9 μm. We highlight a few examples of vesicles in the TEM and NanoSIMS images with red arrows (d) and (e). A blow up of a 2D image showing vesicles in the TEM image, NanoSIMS image, and their overlay is given in Figure S1.

DOI: 10.1021/acsnano.6b07233
ACS Nano XXXX, XXX, XXX−XXX

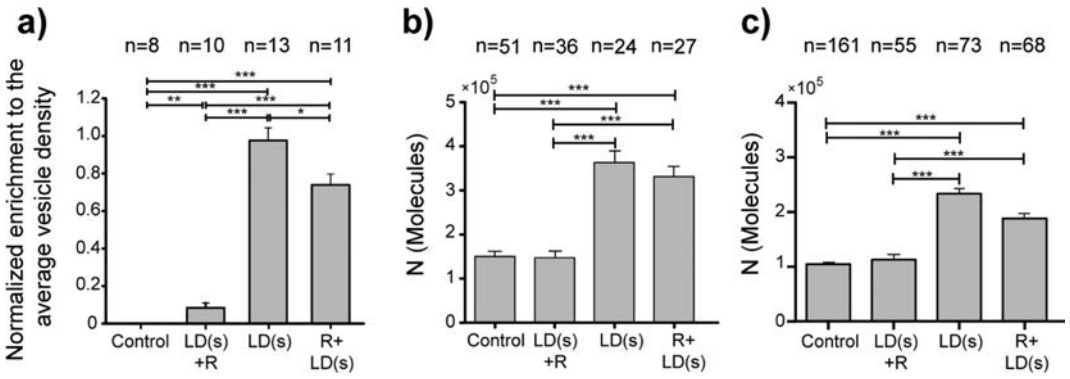

Figure 3. NanoSIMS and electrochemical data for different treatments of PC12 cells. (a) ^{13}C-enrichment normalized to average vesicle density from each group of samples. (b) Number of dopamine molecules detected per vesicle with intracellular electrochemical cytometry. (c) Number of dopamine molecules released per event during exocytosis. Error bars are SEM. One-way ANOVA on ranks: *$p < 0.05$, **$p < 0.01$ and ***$p < 0.001$; n is the number of cells tested. Abbreviations: LD(S), 1.5 h L-DOPA, short exposure; R, reserpine, 1 h exposure.

enriched ^{13}C-dopamine. The observation that dopamine leakage following reserpine appears to occur in a 'last in, first out' manner indicates that there is a labile pool and likewise a retained pool of dopamine within each individual LDCV. Furthermore, to test the competitive VMAT1 inhibition with reserpine, we treated cells with ^{13}C-L-DOPA following reserpine administration (R+LD(S)). Interestingly, we found that ^{13}C-dopamine was localized inside the vesicles, and enrichment was not significantly lower than the sample treated with ^{13}C-L-DOPA only. This suggests that the activity of reserpine is reversible under these conditions and that the percentage of retained molecules following reserpine treatment is fixed.

To further investigate these two pools within single vesicle, we employed two electrochemical techniques, single cell amperometry and intracellular vesicle electrochemical cytometry, which allow quantification of electroactive analytes, in our case dopamine. Single cell amperometry, first introduced by Wightman *et al.*,[23] employs a micrometer-sized electrode that, when placed on the top of a cell, can be used to quantify release from individual exocytosis release events (Figure 1a, top). Intracellular cytometry (Figure 1b, middle), introduced by us is a technique to probe the catecholamine content of single vesicles as they lyse on a nanotip microeloectrode inside of a living cell.[10] In both techniques, vesicular dopamine is released and oxidized at the electrode surface resulting in a peak transient. By applying Faraday's law ($Q = nNF$), it is possible to quantify the oxidation current at the electrode to count the number of dopamine molecules released in moles (N), where Q is the charge that passes through the electrode surface, n is the number of electrons exchanged in a oxidation reaction ($2e^-$ for dopamine), and F is Faraday's constant (96,485 Cmol^{-1}).[28,29]

We first treated two sets of PC12 cells, with ^{12}C- or ^{13}C-L-DOPA, and measured dopamine release with single cell amperometry. This experiment showed no significant difference in the number of molecules released between these cell groups (Figure S2). Therefore, we continued with all electrochemical experiments by treating cells with ^{12}C-L-DOPA. Figure 3b shows data for vesicle dopamine content measured with intracellular electrochemical cytometry, whereas Figure 3c shows the dopamine release data obtained with single cell amperometry. Under control conditions, an average of 124,300 ± 51,700 molecules released per vesicle was measured with single cell amperometry. This value was slightly higher than the previously reported value of 114,300 ± 2105 dopamine molecules[30] and lower than 194,000 ± 13,000 reported by Colliver *et al.*[12] Control PC12 vesicles probed intracellularly contained an average of 152,900 ± 8920 molecules, also higher than previously reported 114,500 ± 15,300 value.[10] In both cases, the difference in measured dopamine content compared with previously reported values might be attributed to differences in culturing and/or experimental conditions. However, we consistently found that the amount released was lower than the amount measured intracellularly in agreement with the concept of partial release.[31]

The PC12 cells used for electrochemical experiments were treated with the same protocols used with NanoSIMS experiments. The electrochemical data largely agreed with the NanoSIMS imaging experiments (Figure 3). We found a statistically significant decrease in dopamine content for the LD(S)+R cells as compared to LD(S) cells. While not statistically different, the R+LD(S) data tend to have a lower dopamine content than that for LD(S) alone. A similar trend in the data among treatment groups compared between these three analytical techniques verifies the quantitative rigor of the NanoSIMS and shows that this method is capable of evaluating the dynamics for accumulation dopamine molecules in individual vesicles. In addition, the electrochemical data show that, in the LD(S)+R experiment, the retained pool contains approximately 140,000 dopamine molecules per vesicle, which is comparable to the control group. Furthermore, we observed that difference between the LD(S)+R and LD(S) experiments was comparatively large. Finally, the comparison between the LD(S) and R+LD(S) experiments showed that preemptively depleting dopamine did not greatly affect the storage capacity of the vesicle.

The bioenergetic and mechanistic aspects of VMAT activity to transport neurotransmitter amines into the vesicle interior, powered by an electrochemical H^+ gradient, have been extensively studied in the last century.[5,32,33] The generally accepted mechanistic view is that VMAT monoamine transport depends on a counter transport of two H^+. The efflux of the first H^+ into cytoplasm generates a high-affinity recognition site for the neurotransmitter. The second H^+ efflux initiates VMAT to undergo a conformational change during which the substrate is moved across the vesicle membrane and released into the vesicle interior. During inhibition of VMAT, reserpine competes for the high-affinity recognition site with monoamine, thus blocking dopamine uptake.[33−36]

DOI: 10.1021/acsnano.6b07233
ACS Nano XXXX, XXX, XXX−XXX

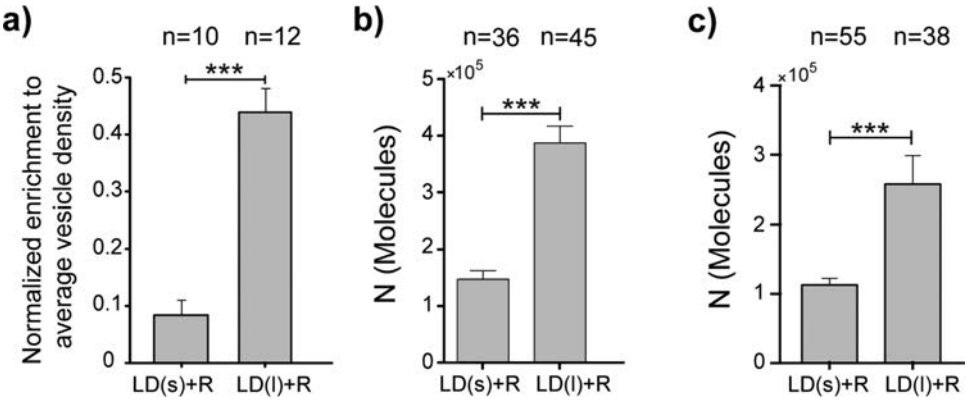

Figure 4. Partitioning of dopamine between vesicular compartments. (a) NanoSIMS measurement of ^{13}C-enrichment, normalized to average vesicle density from each group of samples. (b) Number of dopamine molecules detected per vesicle with intracellular electrochemical cytometry. (c) Number of dopamine molecules released per event during exocytosis. Error bars are SEM. One-way ANOVA on ranks: ***p < 0.001, n is the number of cells tested. Abbreviations: LD(S), 1.5 h L-DOPA, short exposure; LD(L), 12 h L-DOPA, long exposure; R, reserpine, 1 h exposure.

The dopamine depletion in single LDCVs following reserpine administration observed by both NanoSIMS imaging and electrochemical methods apparently results from leakage from the vesicle that is not countered by active transport. It has been reported that vesicles are highly dynamic systems that function with a pump-and-leak mechanism, where the passive leakage of monoamines from vesicle interior is counterbalanced by inward active VMAT transport.[5,12,37,38] If labeled dopamine is evenly distributed and accessible across the vesicle after treatment with labeled L-DOPA, then reserpine-induced leakage should affect both labeled and unlabeled dopamine equally. However, the NanoSIMS observed enrichment of labeled dopamine after loading with L-DOPA decreases almost completely after subsequent blocking of the VMAT with reserpine. This implies that labeled dopamine seems to be leaving the vesicle at a faster rate than the unlabeled dopamine that is already present. The indication is that the halo is an expandable labile pool for dopamine, whereas the dense core is a more tightly regulated, structurally bound pool. We find that the amount of dopamine retained following reserpine treatment is very close to the amount measured in control cells, implying that the function of the halo is probably related to regulation of spikes in cytosolic catecholamine as opposed to dopamine storage *per se*. This leads to the idea of 'last in, first out' regulation of the halo content, a process that allows the halo to exchange catecholamine with the cytosol without adversely affecting the primary function of the vesicle, to store approximately 100,000 dopamine molecules for release.

A Mechanistic View of Vesicle Loading and Nanocopartmentalization. To follow up the observation that dopamine removal occurs at different rates within vesicle compartments, dense core, and halo, we exposed PC12 cells to ^{13}C-L-DOPA for a longer time period (12 h) in an attempt to saturate the vesicular dense core with ^{13}C-dopamine prior to VMAT1 inhibition with reserpine for 1 h (LD(L)+R). Thereafter, cells were analyzed with NanoSIMS, intracellular cytometry, and single cell amperometry, and the results are presented in Figure 4a–c. The normalized enrichment of ^{13}C-dopamine was obtained in the manner described above, and the mean vesicle density for LD(L)+R treated cells is shown in Figure S3. We compared these data with previous results related to the 1.5 h L-DOPA exposure and consequent reserpine treatment (LD(S)+R). In Figure 4a, it is apparent that there is greater enrichment in the retained pool for 12 h L-DOPA incubation, LD(L)+R, when compared to the LD(S)+R. Interestingly we found that the number of molecules retained increased following the long incubation (p < 0.001), and this was confirmed with the quantitative electrochemical analysis for both vesicle content and exocytosis release (Figure 4b, c). These data show that dopamine depletion by reserpine is less effective when PC12 cells are treated with ^{13}C L-DOPA for the longer 12 h time period, indicating that the dense core moiety has a role in entrapping loaded dopamine and it is not just a means to electrostatically stabilize the vesicular solution.

In these experiments it became apparent that we were not significantly diminishing the retained pool because the halo was acting as a kinetic buffer. This led us to the experiments with L-DOPA exposure for 12 h, which showed that vesicles are more enriched when exposed for longer time. The mechanism proposed is consistent with the storage mechanism proposed by Oleinick *et al.*,[39] where dopamine during 12 h L-DOPA exposure occupies not only the halo solution but also penetrates into spaces between highly compacted nodules of chromogranin proteins that constitute the dense core (Figure 5c). When the cells are post-treated with reserpine, they show slower kinetics of dopamine leakage because it requires a larger activation energy for dopamine to diffuse from the dense core to the halo compartment prior to moving from the halo across the vesicle membrane into the cytoplasm. This is evidenced by the increased ^{13}C-dopamine enrichment observed in the 12 h incubation of L-DOPA and subsequent incubation with reserpine. The electrochemical data also show that more molecules are retained, but the ratio for enrichment in the NanoSIMS experiment is much greater than for the electrochemically determined total content again in agreement with a nanocompartmentalization. Thus, the longer incubation time has apparently increased the number of catecholamine molecules within the dense core. Likewise, and due to the reduced leakage kinetics in this matrix, a larger number of molecules is retained following reserpine treatment.

Although it has been reported that VMAT is irreversibly blocked by reserpine,[34,35] the sets of experiments during which reserpine was administrated first, followed by L-DOPA treatment, clearly show that reserpine has a reversible effect on VMAT1. This suggests that a competitive inhibition mechanism is more likely. During the 1950s, Carlsson *et al.*

DOI: 10.1021/acsnano.6b07233
ACS Nano XXXX, XXX, XXX–XXX

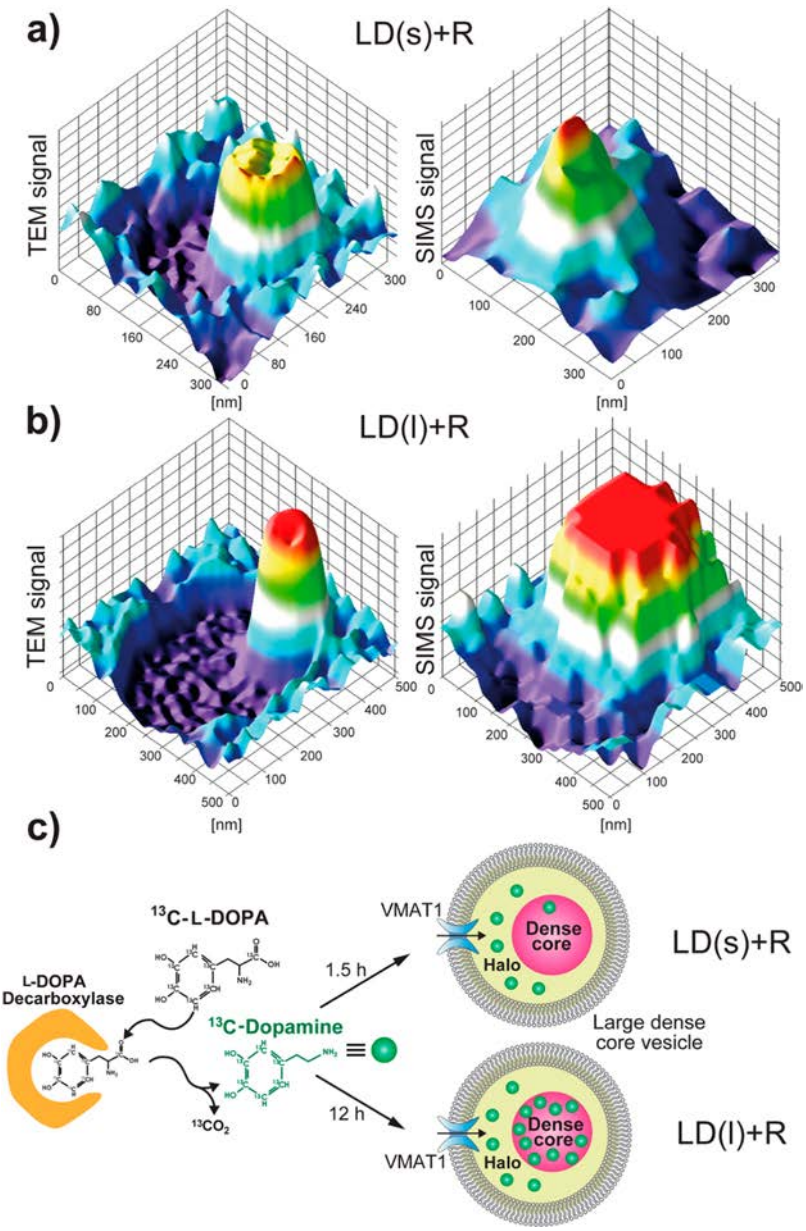

Figure 5. Correlation between TEM and NanoSIMS images of single vesicle allows dopamine localization in vesicular compartments. 3D surface plots of TEM (left) and $^{13}C^{14}N^-$ ion species NanoSIMS imaging (right) for: (a) short L-DOPA exposure following reserpine treatment (LD(S)+R) and (b) long L-DOPA exposure following reserpine treatment (LD(L)+R). (c) Model for dopamine distribution across the vesicle after short and long exposure with L-DOPA (dopamine is in green). Abbreviations: LD(S), 1.5 h L-DOPA, short exposure; LD(L), 12 h L-DOPA, long exposure; R, reserpine, 1 h exposure.

showed that treatment of mice with reserpine makes them completely sedated, and this could be reversed after L-DOPA administration,[40] suggesting the reversibility of reserpine inhibition under certain conditions and supporting our observations. Moreover, studies in rat brain have shown that a moderate elevation of dopamine and norepinephrine in cytoplasm *via* blocking the metabolic enzyme monoamine oxidase is sufficient to inhibit reserpine action when subsequently administrated.[8]

Combined TEM and NanoSIMS Analyses Allow Dopamine Localization in Vesicle Nanocompartments. Vesicles clearly have a high loading capacity during long L-DOPA incubation (Figure 5). It is generally thought that the added capacity is a result of dopamine storage in the dense core, but our observations above suggest this is rate limited. To acquire more insight into the spatial dopamine distribution within the vesicle interior, we performed further image analysis by correlating TEM and SIMS data to discriminate the content of the nanometer dense core from the halo.

It has been reported that control PC12 vesicles have a mean diameter around 192 nm,[12,41] whereas L-DOPA treated vesicles are somewhat larger with a mean diameter of 254 nm.[41] NanoSIMS can achieve a lateral beam resolution of 50 nm,[19] and TEM can achieve approximately 400 times better spatial resolving power.[42] Thus, in this analysis, the limit of the NanoSIMS spatial imaging capabilities was complemented by correlating to TEM images to provide a rare view of the distribution of dopamine within the LDCV. Figure 5 shows an example of a color-coded 3D surface plot from a TEM and a NanoSIMS image of the same vesicle. Here we focus on data

DOI: 10.1021/acsnano.6b07233
ACS Nano XXXX, XXX, XXX−XXX

analysis for two treatments: 1.5 h of ^{13}C-L-DOPA followed by reserpine (LD(S)+R; Figure 5a) and 12 h of ^{13}C-L-DOPA followed by reserpine (LD(L)+R; Figure 5b). For the TEM data (on the left), yellow and red signals are attributed to the dense core protein localization, whereas the dark blue shows the halo. The corresponding NanoSIMS intensity plots, in each case from the same individual vesicle as the corresponding TEM image, are shown on the right. Here, the dark blue and red show lower and higher signal intensity for $^{13}C^{14}N^-$ ion species, respectively. In Figure 5a, the single vesicle SIMS plot reveals that a 1.5 h L-DOPA treatment followed by reserpine allows dopamine to occupy only a part of the vesicle interior, and the TEM data show that it is mostly associated with the halo compartment. In contrast, a 12 h exposure to L-DOPA and then reserpine shows the capacity of the dense core to capture larger amounts of dopamine. This is evident in Figure 5b, as dopamine enrichment is present in both the dense core and halo. The trend in the levels of dopamine is consistent with the semiquantitative data obtained with NanoSIMS, the quantitative electrochemical vesicle impact cytometry data, and electrochemical measurements of release, but the observation in this image example suggests that this is compartment specific at the nanometer level.

From these remarkable images, we again suggest that vesicle compartments are separated *via* a thermodynamic driving force that limits dopamine movement between them. As the halo is between the dense core and the vesicle membrane, it appears to act as a kinetic buffer for dopamine moving from the dense core to the vesicle membrane. This supports the hypothesis of Marszalek *et al.*[43] that ion exchange regulates amine transfer between dense core and halo, and this is only possible to discern now by use of the NanoSIMS and TEM combined approach and the quantitative correlation with electrochemical content of vesicles and release. In the future, correlating TEM and the NanoSIMS quantitative data across the nanometer vesicle might be directly obtained.

CONCLUSIONS

In this work we show that NanoSIMS isotopic imaging permits to look into and spatially resolve the chemistry across nanometer-sized transmitter vesicles. The combination with nanoelectrochemical methods provides a means to quantify and relate vesicle content and release, and we used this to determine that dopamine transfer between the nanometer vesicular compartments is kinetically limited. Combining TEM with NanoSIMS, we have obtained some astounding images and are able to show profiles of dopamine across single vesicles. From this approach, we have been able to go into vesicles and study processes at the single vesicle level that are difficult or impossible to examine with larger scale methods, like the partitioning of dopamine storage across the compartments of an individual vesicle. Interestingly, patch clamp experiments suggest that serotonin is preferentially released from the vesicular halo in mast cell vesicles in modes of release where only part of the vesicle cargo has been released.[44] Examining the concentrations of catecholamine across these compartments in our system and comparing to the spatial distribution, when treated for hours with L-DOPA, suggest that the thermodynamics to translocate these amines across the nanometer dense core is extremely large.

METHODS

Cell Culture. PC12 cells donated by Lloyd Greene (Columbia University, USA) were cultured as previously described.[45] In brief, cells were grown on collagen IV coated culture dishes and subcultured every 7−9 days. The maintenance of cells was done at 37 °C in a water saturated atmosphere containing 7% CO_2 and in culture medium composed of L-glutamine and phenol red free RPMI 1640 (Lonza, Fisher Scientific, Sweden) supplemented with 10% horse and 5% fetal bovine serums (Sigma-Aldrich, Sweden). Culture media was replaced every 2−3 days. For NanoSIMS experiments, cells were plated in collagen IV coated T-75 flasks (Falcon, Fisher Scientific, Sweden) with approximately 2.2 million cells per flask and cultured for 5−6 days until obtaining uniform cell monolayer. Cells were cultured for electrochemical experiments in collagen IV-coated 60 mm dishes (Corning, VWR, Sweden) with approximately 100,000 cells per dish for 3−4 days before experiments.

Experimental Design. Cells were treated with stable isotope-labeled L-3,4-dihydroxyphenylalanine (L-DOPA (1−13C, RING-13C6, 99%, Cambridge Isotope Laboratories Inc., MA, USA) for NanoSIMS experiments, L-DOPA (Sigma-Aldrich, Sweden) for electrochemical experiments, and reserpine (Sigma-Aldrich, Sweden) or consequent treatment with stable isotope labeled L-DOPA (or L-DOPA), and reserpine was applied. In the case of L-DOPA in general, a stock solution was prepared by dissolving L-DOPA in phosphate buffered saline, PBS (Sigma-Aldrich, Sweden), in the dark and simultaneously purging with argon (6.0, AGA Sweden) due to the L-DOPA sensitivity toward oxygen. A final L-DOPA solution with a concentration of 150 μM was obtained by diluting stock solution in warm cell media. Cells were treated for 90 min (short exposure) or 12 h (long exposure). In the case of reserpine, the stock solution was made in DMSO (Sigma-Aldrich, Sweden). Cells were treated for 1 h with a final reserpine concentration of 1 μM prepared in warm cell media. To prevent DMSO toxicity on cells in culture, we used final reserpine solutions having 0.05% (v/v) DMSO and osmolality 289 mOsm/kg, therefore, the negative effect of DMSO on cell viability was excluded. In the case of the consequent treatments, cells were washed two times with warm cell media before the next drug exposure. All treatments were performed in an incubator at 37 °C in water saturated atmosphere containing 5% CO_2. For NanoSIMS experiments, the treated cells were washed two times with Dulbecco's phosphate buffered saline without calcium and magnesium (Sigma-Aldrich, Sweden), enzymatically harvested with TrypLE Express (GIBCO, Fisher Scientific, Sweden), and resuspended in PBS for subsequent chemical fixation. Electrochemical measurements were carried out on treated cells after rinsing two times with warm (37 °C) isotonic saline buffer (150 mM NaCl, 5 mM KCl, 1.2 mM $MgCl_2$, 2 mM $CaCl_2$, 5 mM glucose, 10 mM HEPES, pH 7.4) and aliquoting 5 mL of isotonic saline into the dish. The sample was placed on an inverted microscope (IX71 or IX81, Olympus) with a heat stage held at 37 °C, where the amperometric measurements were performed. The cell studies were reproduced on 3 different PC12 cell generations for both NanoSIMS imaging, and the electrochemical analyses (total number of analyzed cells, *n*, are indicated in Figures 3 and 4 and relevant Supporting Figures).

Chemical Fixation and Embedding. Cell suspensions were incubated at 4 °C overnight with modified Karnovsky fixative[46] containing 0.01% sodium azide (BDH, UK), 1% formaldehyde (Sigma-Aldrich, Sweden), and 1.25% glutaraldehyde (Agar Scientific Ltd., UK). Afterward, cells were washed with 150 mM sodium cacodylate buffer (Agar Scientific Ltd., UK) and postfixed with 1% osmium tetroxide (Agar Scientific Ltd., UK) at 4 °C for 2 h and 0.5% uranyl acetate (Merck, Sigma-Aldrich, Sweden) at room temperature in dark for 1 h. Dehydration was done with rising concentrations of ethanol (70%, 85%, 95% and 99.5%) and later with 100% acetone and embedded in Agar 100 resin (Agar Scientific Ltd., UK). Sections, 70 nm thick, were obtained with an ultramicrotome (Leica EM UC6), placed onto Formvar coated copper grids (FCF200F1−Cu, EMS, USA), and poststained with uranyl acetate and Reynolds lead citrate.[47]

DOI: 10.1021/acsnano.6b07233
ACS Nano XXXX, XXX, XXX−XXX

Transmission electron Microscopy. Prior to NanoSIMS imaging, electron microscopy observations were carried out with a Leo 912AB Omega microscope (Center for Cellular Imaging, Sahlgrenska Academy, University of Gothenburg) operated at 120 kV.

NanoSIMS Imaging. High-resolution secondary ion maps were acquired from the same ultrathin sections used for TEM imaging with a NanoSIMS 50L ion microprobe (CAMECA, France) at the Chemical Imaging Infrastructure at Chalmers University of Technology and University of Gothenburg. Prior to imaging, implantation of Cs^+ ions was done by scanning the area of interest with a defocused primary ion beam (aperture diaphragm: D1-1, the beam current value was between 5.4 pA and 8 pA, and field of view 40 × 40 μm^2) for 1 min. Focused 16 keV Cs^+ primary ions were then scanned across the sample surface to obtain high-spatial resolution negative ion images. Primary ion beam current was measured at the sample site and had values between 0.35 pA and 0.98 pA. Images were acquired at a resolution 256 × 256 pixels with a fields of view between 8 × 8 μm^2 and 12 × 12 μm^2 and a dwell time of 5 ms/pixel, taking approximately 5 min per image layer. Ion maps were acquired for the $^{12}C^{14}N^-$ and $^{13}C^{14}N^-$ ion species at a mass resolution of 9000 (Cameca definition), sufficient to resolve potential molecular interferences. Final images typically contained 2−8 image planes.

Image Data Processing. The NanoSIMS images in Figure 2 were processed using the ImageJ plugin OpenMIMS (v 2.5 (rev: 713); MIMS, Harvard University; http://www.nrims.hms.harvard.edu/). Sequential image planes were collected, drift corrected, and added, and $^{13}C^{14}N^-/^{12}C^{14}N^-$ ratio maps were made as a hue-saturation-intensity image (HSI) with a linear color scale showing lower isotopic ratios in dark blue and higher ratios in red and yellow. Signal filtering was done with a median filter with 0.5 pixel radius. Surface plots for TEM and SIMS images were produced using the ImageJ freeware software (https://imagej.nih.gov/ij/) 3D Surface Plot tool, where the $^{13}C^{14}N^-$ NanoSIMS maps and the TEM signal (opacity) were plotted on the *z*-axis. The plots were rotated 45° about the *x*- and *z*-axes to better display the profile of each signal. MATLAB R2016a (Mathworks Inc., Natick, MA) was used to obtain quantitative data and ratio images. Initially all raw data (.im) files were preprocessed and imported using the Look@NanoSIMS plugin.[48] Further data processing to generate ratio images and enriched vesicle detection was done with an in-house written routine (available upon request). The work flow of the routine was as follows: Initially all images were filtered using a median filter (3 × 3 pixels), and later a region of interest (ROI-1) containing the cell was determined from the $^{13}C^{14}N^-/^{12}C^{14}N^-$ ratio image. Subsequently a second region of interest (ROI-2) not containing any vesicles was assigned within ROI-1. ROI-2 contains the background and from this the natural abundance $^{13}C^{14}N^-/^{12}C^{14}N^-$ ratio (*NA*) was determined. After that ratio images were generated using the following equation:

$$\text{ratio} = \frac{^{13}C^{14}N}{^{12}C^{14}N} - NA$$

The ratio of the ^{13}C and ^{12}C signal is subtracted with natural abundancy (*NA*) and provides images with regions of enriched ^{13}C having a positive value, whereas regions not enriched in ^{13}C are assigned a value of zero. Enriched vesicles were automatically assigned using the following criteria: 9 connected neighboring pixels within in ROI-1 with a signal larger than 3× the standard deviation of the background (*NA*). For each vesicle, the average enrichment was calculated. The density of enriched vesicles was determined by dividing the number of observed enriched vesicles with the area of ROI-1, giving the vesicle density as number of vesicles per μm^2. The average vesicle enrichment per cell was normalized to the average vesicle density per group to obtain Figures 3a, 4a, and S4.

Single Cell Amperometry. Electrodes were prepared by aspirating a 5 μm carbon fiber into a glass capillary (B120-69-10, Sutter Instrument Co., Novato, CA). A micropipette puller (P-1000, Sutter Instruments Co.) was used to divide the capillary into two narrow tip pipettes. The extended carbon fiber was cut close to the end of the glass. The electrodes were sealed by dipping the tips into epoxy (Epoxy Technology Inc., Billerica, MA) and cured overnight at 100 °C. Before the measurement, the electrodes were bevelled at a 45° angle, backfilled with 3 M KCl, and tested in a 100 μM dopamine solution. Only electrodes with stable and symmetrical cyclic voltammograms were used for the experiments (−0.2 to 0.8 V *vs* a AglAgCl, at scan rate 100 mV/s). For data collection, a commercial patch-clamp instrument (Axopatch 200B, Axon Instruments, Foster City, CA) and a digital acquisition system (Digidata 1440A, Axon Instruments) were used. The electrode was held at +700 mV *vs* a AglAgCl reference electrode and placed on top of a cell using a micromanipulator. The signal was acquired at 10 kHz and filtered at 2 kHz using a 4-pole Bessel filter. After collecting 5 s of baseline, cells were stimulated for 5 s using a micropipette filled with a high-concentration potassium solution (55 mM NaCl, 100 mM KCl, 1.2 mM $MgCl_2$, 2 mM $CaCl_2$, 5 mM glucose, 10 mM HEPES). Each cell was stimulated 3 times, allowing 60 s recovery between stimulations. The data were analyzed in Igor Pro 6 (version 6.36, WaveMetrics, Lake Oswego, OR) with a macro written by Mosharov and Sulzer.[49] Traces were smoothed using a 1 kHz binomial filter, and peaks were detected above a threshold of 5 times the RMS noise. Statistical analysis was done with Kruskal−Wallis test in MATLAB (MathWorks Inc.).

Intracellular Vesicle Electrochemical Cytometry. Nanotip conical carbon fiber microelectrodes were prepared as previously described.[10,50] Briefly, 5 μm carbon fibers were aspirated into glass capillaries and pulled as above, except a Sutter Instruments Co. puller (Novato, CA) was used. The carbon fiber extending from the glass capillary was cut to approximately 100−150 μm length and flame etched. The electrodes obtained had needle-sharp fiber tips with approximately 50−100 nm diameter and 30−100 μm length. After sealing with epoxy (Epoxy Technology), each electrode was backfilled with 3 M KCl and tested in a 100 μM dopamine solution over a potential window of −0.2 to +0.8 V *vs* a AglAgCl reference electrode, at a scan rate of 100 mV/s. Only electrodes with stable and symmetrical cyclic voltammograms were used for the experiments. Cellular electrochemical recordings were performed as previously described,[10] and described above, except the output was filtered at 2 kHz with a low pass 4-pole Bessel filter and digitized at 5 kHz. After data acquisition, each microelectrode was tested in 100 μM dopamine solution, and only data obtained with electrodes with unchanged cyclic voltammogram were used. Peaks below a threshold of 3× the RMS noise were discarded. The data were analyzed and statistically treated in the same manner as the single cell amperometry data described above.

ASSOCIATED CONTENT

Supporting Information

The Supporting Information is available free of charge on the ACS Publications website at DOI: 10.1021/acsnano.6b07233.

Figure S1: A blow up of a 2D image showing single vesicle in the overlay of TEM image and NanoSIMS $^{13}C^{14}N^-/^{12}C^{14}N^-$ ratio image. Figure S2: Investigation of the impact of isotopically labeled L-DOPA on dopamine release from cells. Figure S3: Vesicle density for treated samples. Figure S4: NanoSIMS enrichment data for control experiments of reserpine impact to vesicle leakage. Figure S5: Vesicle density for samples treated with cell media compared to L-DOPA-reserpine treatments. Figure S6: Cell response data for different treatments of PC12 cells obtained by electrochemical techniques. Figure S7: NanoSIMS $^{13}C^{14}N^-/^{12}C^{14}N^-$ ratio images of a PC12 cell exposed to ^{13}C-L-DOPA for 1.5 h (PDF)

DOI: 10.1021/acsnano.6b07233
ACS Nano XXXX, XXX, XXX−XXX

AUTHOR INFORMATION

Corresponding Author

*E-mail: andrew.ewing@chem.gu.se.

ORCID

Michael E. Kurczy: 0000-0001-6579-9691

Andrew G. Ewing: 0000-0002-2084-0133

Notes

The authors declare no competing financial interest.

ACKNOWLEDGMENTS

We acknowledge the Centre for Cellular Imaging at the Sahlgrenska Academy, University of Gothenburg for the use of transmission electron microscope and for support from the staff. This research was funded by the Swedish Research Council (2015-05274), The Knut and Alice Wallenberg Foundation (2015.0341), and the USA National Institutes of Health (NIH). The NanoSIMS work was carried out with the Infrastructure for chemical imaging at the University of Gothenburg and Chalmers University of Technology, located at the Astra Zeneca BioVenture Hub.

REFERENCES

(1) Meldolesi, J.; Ceccarelli, B. Exocytosis and Membrane Recycling. *Philos. Trans. R. Soc., B* **1981**, *296*, 55−65.

(2) Burgoyne, R. D.; Morgan, A. Secretory Granule Exocytosis. *Physiol. Rev.* **2003**, *83*, 581−632.

(3) Hide, I.; Bennett, J. P.; Pizzey, A.; Boonen, G.; Bar-Sagi, D.; Gomperts, B. D.; Tatham, P. E. Degranulation of Individual Mast Cells in Response to Ca^{2+} and Guanine Nucleotides: An All-Or-None Event. *J. Cell Biol.* **1993**, *123*, 585−593.

(4) An, S.; Zenisek, D. Regulation of Exocytosis in Neurons and Neuroendocrine Cells. *Curr. Opin. Neurobiol.* **2004**, *14*, 522−530.

(5) Edwards, R. H. The Neurotransmitter Cycle and Quantal Size. *Neuron* **2007**, *55*, 835−858.

(6) Liu, Y.; Edwards, R. H. Differential Localization of Vesicular Acetylcholine and Monoamine Transporters in PC12 Cells but not CHO Cells. *J. Cell Biol.* **1997**, *139*, 907−916.

(7) Peter, D.; Liu, Y.; Sternini, C.; de Giorgio, R.; Brecha, N.; Edwards, R. H. Differential Expression of Two Vesicular Monoamine Transporters. *J. Neurosci.* **1995**, *15*, 6179−6188.

(8) Varoqui, H.; Erickson, J. D. Vesicular Neurotransmitter Transporters. *Mol. Neurobiol.* **1997**, *15*, 165−191.

(9) Dunevall, J.; Fathali, H.; Najafinobar, N.; Lovric, J.; Wigström, J.; Cans, A.-S.; Ewing, A. G. Characterizing the Catecholamine Content of Single Mammalian Vesicles by Collision−Adsorption Events at an Electrode. *J. Am. Chem. Soc.* **2015**, *137*, 4344−4346.

(10) Li, X.; Majdi, S.; Dunevall, J.; Fathali, H.; Ewing, A. G. Quantitative Measurement of Transmitters in Individual Vesicles in the Cytoplasm of Single Cells with Nanotip Electrodes. *Angew. Chem., Int. Ed.* **2015**, *54*, 11978−11982.

(11) Yao, J.; Erickson, J. D.; Hersh, L. B. Protein Kinase A Affects Trafficking of the Vesicular Monoamine Transporters in PC12 Cells. *Traffic* **2004**, *5*, 1006−1016.

(12) Colliver, T. L.; Pyott, S. J.; Achalabun, M.; Ewing, A. G. VMAT-Mediated Changes in Quantal Size and Vesicular Volume. *J. Neurosci.* **2000**, *20*, 5276−5282.

(13) Greene, L. A.; Rein, G. Release, Storage and Uptake of Catecholamines by a Clonal Cell Line of Nerve Growth Factor (NGF) Responsive Pheochromocytoma Cells. *Brain Res.* **1977**, *129*, 247−263.

(14) Kittner, B.; Bräutigam, M.; Herken, H. PC12 Cells: a Model System for Studying Drug Effects on Dopamine Synthesis and Release. *Arch. Int. Pharmacodyn. Ther.* **1987**, *286*, 181−194.

(15) Kozminski, K. D.; Gutman, D. A.; Davila, V.; Sulzer, D.; Ewing, A. G. Voltammetric and Pharmacological Characterization of Dopamine Release from Single Exocytotic Events at Rat Pheochromocytoma (PC12) Cells. *Anal. Chem.* **1998**, *70*, 3123−3130.

(16) Gong, L. W.; Hafez, I.; Alvarez de Toledo, G.; Lindau, M. Secretory Vesicles Membrane Area is Regulated in Tandem with Quantal Size in Chromaffin Cells. *J. Neurosci.* **2003**, *23*, 7917−7921.

(17) Mundorf, M. L.; Troyer, K. P.; Hochstetler, S. E.; Near, J. A.; Wightman, R. M. Vesicular Ca^{2+} Participates in the Catalysis of Exocytosis. *J. Biol. Chem.* **2000**, *275*, 9136−9142.

(18) Ahmed, S.; Titchmarsh, J. M.; Kilburn, M. R.; Grovenor, C. R. M. Examination of the Influence of Boron on the Microstructure and Properties of Low C Ferritic Steels Using NanoSIMS and TEM. *Appl. Surf. Sci.* **2006**, *252*, 7062−7065.

(19) Hoppe, P.; Cohen, S.; Meibom, A. NanoSIMS: Technical Aspects and Applications in Cosmochemistry and Biological Geochemistry. *Geostand. Geoanal. Res.* **2013**, *37*, 111−154.

(20) Boxer, S. G.; Kraft, M. L.; Weber, P. K. Advances in Imaging Secondary Ion Mass Spectrometry for Biological Samples. *Annu. Rev. Biophys.* **2009**, *38*, 53−74.

(21) Steinhauser, M. L.; Bailey, A. P.; Senyo, S. E.; Guillermier, C.; Perlstein, T. S.; Gould, A. P.; Lee, R. T.; Lechene, C. P. Multi-Isotope Imaging Mass Spectrometry Quantifies Stem Cell Division and Metabolism. *Nature* **2012**, *481*, 516−519.

(22) Wedlock, L. E.; Kilburn, M. R.; Liu, R.; Shaw, J. A.; Berners-Price, S. J.; Farrell, N. P. NanoSIMS Multi-Element Imaging Reveals Internalisation and Nucleolar Targeting for a Highly-Charged Polynuclear Platinum Compound. *Chem. Commun.* **2013**, *49*, 6944−6946.

(23) Wightman, R. M.; Jankowski, J. A.; Kennedy, R. T.; Kawagoe, K. T.; Schroeder, T. J.; Leszczyszyn, D. J.; Near, J. A.; Diliberto, E. J.; Viveros, O. H. Temporally Resolved Catecholamine Spikes Correspond to Single Vesicle Release from Individual Chromaffin Cells. *Proc. Natl. Acad. Sci. U. S. A.* **1991**, *88*, 10754−10758.

(24) Takado, Y.; Knott, G.; Humbel, B. M.; Escrig, S.; Masoodi, M.; Meibom, A.; Comment, A. Imaging Liver and Brain Glycogen Metabolism at the Nanometer Scale. *Nanomedicine* **2015**, *11*, 239−245.

(25) Brismar, H.; Aperia, A.; Westin, L.; Moy, J.; Wang, M.; Guillermier, C.; Poczatek, J. C.; Lechene, C. Study of Protein and RNA in Dendritic Spines Using Multi-Isotope Imaging Mass Spectrometry. *Surf. Interface Anal.* **2014**, *46*, 158−160.

(26) Audinot, J.-N.; Georgantzopoulou, A.; Piret, J.-P.; Gutleb, A. C.; Dowsett, D.; Migeon, H. N.; Hoffmann, L. Identification and Localization of Nanoparticles in Tissues by Mass Spectrometry. *Surf. Interface Anal.* **2013**, *45*, 230−233.

(27) Ouellette, R. J.; Rawn, J. D. 23 - Amines and Amides. In *Organic Chemistry*; Elsevier: Boston, 2014; pp 803−842.

(28) Mellander, L.; Cans, A.-S.; Ewing, A. G. Electrochemical Probes for Detection and Analysis of Exocytosis and Vesicles. *ChemPhysChem* **2010**, *11*, 2756−2763.

(29) Cans, A.-S.; Ewing, A. G. Highlights of 20 Years of Electrochemical Measurements of Exocytosis at Cells and Artificial Cells. *J. Solid State Electrochem.* **2011**, *15*, 1437−1450.

(30) Chen, T. K.; Luo, G.; Ewing, A. G. Amperometric Monitoring of Stimulated Catecholamine Release from Rat Pheochromocytoma (PC12) Cells at the Zeptomole Level. *Anal. Chem.* **1994**, *66*, 3031−3035.

(31) Ren, L.; Mellander, L. J.; Keighron, J.; Cans, A.-S.; Kurczy, M. E.; Svir, I.; Oleinick, A.; Amatore, C.; Ewing, A. G. The Evidence for Open and Closed Exocytosis as the Primary Release Mechanism. *Q. Rev. Biophys.* **2016**, *49*, e12.

(32) Johnson, R. G., Jr. Accumulation of Biological Amines into Chromaffin Granules: A Model for Hormone and Neurotransmitter Transport. *Physiol. Rev.* **1988**, *68*, 232−307.

(33) Schuldiner, S.; Shirvan, A.; Linial, M. Vesicular Neurotransmitter Transporters: from Bacteria to Humans. *Physiol. Rev.* **1995**, *75*, 369−392.

(34) Schuldiner, S.; Liu, Y.; Edwards, R. H. Reserpine Binding to a Vesicular Amine Transporter Expressed in Chinese Hamster Ovary Fibroblasts. *J. Biol. Chem.* **1993**, *268*, 29−34.

(35) Rudnick, G.; Steiner-Mordoch, S. S.; Fishkes, H.; Stern-Bach, Y.; Schuldiner, S. Energetics of Reserpine Binding and Occlusion by the

DOI: 10.1021/acsnano.6b07233
ACS Nano XXXX, XXX, XXX−XXX

Chromaffin Granule Biogenic Amine Transporter. *Biochemistry* **1990**, *29*, 603−608.
(36) Chaudhry, F. A.; Boulland, J. L.; Jenstad, M.; Bredahl, M. K.; Edwards, R. H. Pharmacology of Neurotransmitter Transport into Secretory Vesicles. *Handb. Exp. Pharmacol.* **2008**, *184*, 77−106.
(37) Eisenhofer, G.; Kopin, I. J.; Goldstein, D. S. Leaky Catecholamine Stores: Undue Waste or a Stress Response Coping Mechanism? *Ann. N. Y. Acad. Sci.* **2004**, *1018*, 224−230.
(38) Shore, P. A. The Mechanism of Norepinephrine Depletion by Reserpine, Metaraminol and Related Agents. The Role of Monoamine Oxidase. *Pharmacol. Rev.* **1966**, *18*, 561−568.
(39) Oleinick, A.; Hu, R.; Ren, B.; Tian, Z.-Q.; Svir, I.; Amatore, C. Theoretical Model of Neurotransmitter Release During *in Vivo* Vesicular Exocytosis Based on a Grainy Biphasic Nano-Structuration of Chromogranins within Dense Core Matrixes. *J. Electrochem. Soc.* **2016**, *163*, H3014−H3024.
(40) Carlsson, A.; Lindqvist, M.; Magnusson, T. 3,4-Dihydroxyphenylalanine and 5-Hydroxytryptophan as Reserpine Antagonists. *Nature* **1957**, *180*, 1200.
(41) Sombers, L. A.; Hanchar, H. J.; Colliver, T. L.; Wittenberg, N.; Cans, A.; Arbault, S.; Amatore, C.; Ewing, A. G. The Effects of Vesicular Volume on Secretion Through the Fusion Pore in Exocytotic Release from PC12 Cells. *J. Neurosci.* **2004**, *24*, 303−309.
(42) Bozzola, J. J. Electron Microscopy. In *eLS*; John Wiley & Sons, Ltd: Chichester, U.K., 2001.
(43) Marszalek, P. E.; Farrell, B.; Verdugo, P.; Fernandez, J. M. Kinetics of Release of Serotonin from Isolated Secretory Granules. II. Ion Exchange Determines the Diffusivity of Serotonin. *Biophys. J.* **1997**, *73*, 1169−1183.
(44) de Toledo, G. A.; Fernandez-Chacon, R.; Fernandez, J. M. Release of Secretory Products During Transient Vesicle Fusion. *Nature* **1993**, *363*, 554−558.
(45) Banker, G.; Goslin, K. Culturing Nerve Cell. *J. Neuropathol. Exp. Neurol.* **1999**, *58*, 312.
(46) Karnovsky, M. J. A Formaldehyde-Glutaraldehyde Fixative of High Osmolality for Use in Electron Microscopy. *J. Cell Biol.* **1965**, *27*, 137−138A.
(47) Reynolds, E. S. The Use of Lead Citrate at High pH As an Electron-Opaque Stain in Electron Microscopy. *J. Cell Biol.* **1963**, *17*, 208−212.
(48) Polerecky, L.; Adam, B.; Milucka, J.; Musat, N.; Vagner, T.; Kuypers, M. M. Look@NanoSIMS-a Tool for the Analysis of NanoSIMS Data in Environmental Microbiology. *Environ. Microbiol.* **2012**, *14*, 1009−1023.
(49) Mosharov, E. V.; Sulzer, D. Analysis of Exocytotic Events Recorded by Amperometry. *Nat. Methods* **2005**, *2*, 651−658.
(50) Strein, T. G.; Ewing, A. G. Characterization of Submicron-Sized Carbon Electrodes Insulated with a Phenol-Allylphenol Copolymer. *Anal. Chem.* **1992**, *64*, 1368−1373.

DOI: 10.1021/acsnano.6b07233
ACS Nano XXXX, XXX, XXX−XXX

Supporting Information

Nano Secondary Ion Mass Spectrometry Imaging of Dopamine Distribution Across Nanometer Vesicles

Jelena Lovrić[1,2], Johan Dunevall[1], Anna Larsson[3], Lin Ren[1], Shalini Andersson[4], Anders Meibom[5], Per Malmberg[1,2], Michael E. Kurczy[4] & Andrew G. Ewing[1,2,3]

[1]Department of Chemistry and Chemical Engineering, Chalmers University of Technology, SE-412 96 Gothenburg, Sweden. [2]National Centre for Imaging Mass Spectrometry, Chalmers University of Technology and University of Gothenburg, SE-412 96 Gothenburg, Sweden. [3]Department of Chemistry and Molecular Biology, University of Gothenburg, SE-412 96 Gothenburg, Sweden. [4]Cardiovascular and Metabolic Diseases, Innovative Medicines and Early Development Biotech Unit, AstraZeneca, SE-431 50 Mölndal, Sweden. [5]Laboratory for Biological Geochemistry, École Polytechnique Fédérale de Lausanne and Center for Advanced Surface Analysis, Institute of Earth Sciences, University of Lausanne, CH-1015, Lausanne, Switzerland.

Supporting Figures

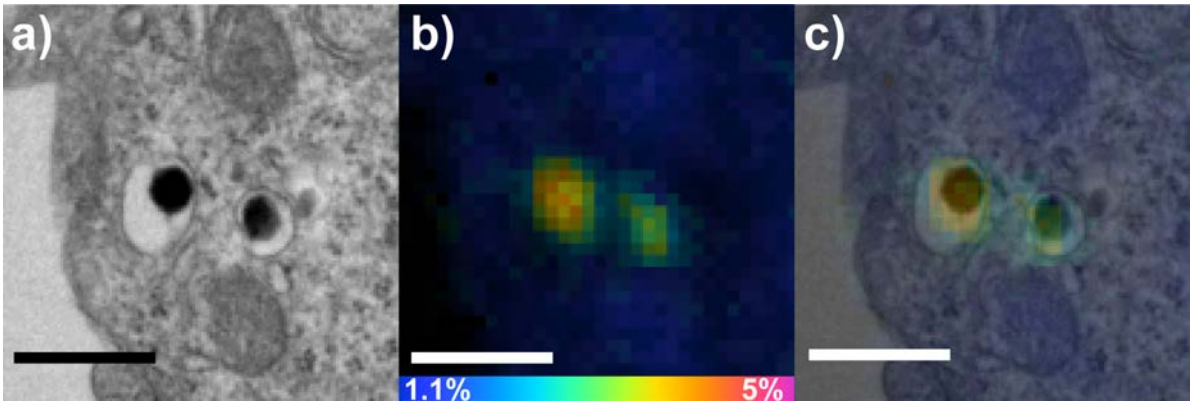

Figure S1. A blow up of a 2D image showing vesicles in: (a) TEM image; (b) Hue-saturation-intensity (HSI) image of the quantified $^{13}C^{14}N^{-}/^{12}C^{14}N^{-}$ isotopic ratio. The dark blue and red on color coded bar show lower and higher isotopic enrichment in ^{13}C- dopamine, respectively; (c) the overlay of TEM and NanoSIMS isotopic ratio image. Scale bar: 500 nm.

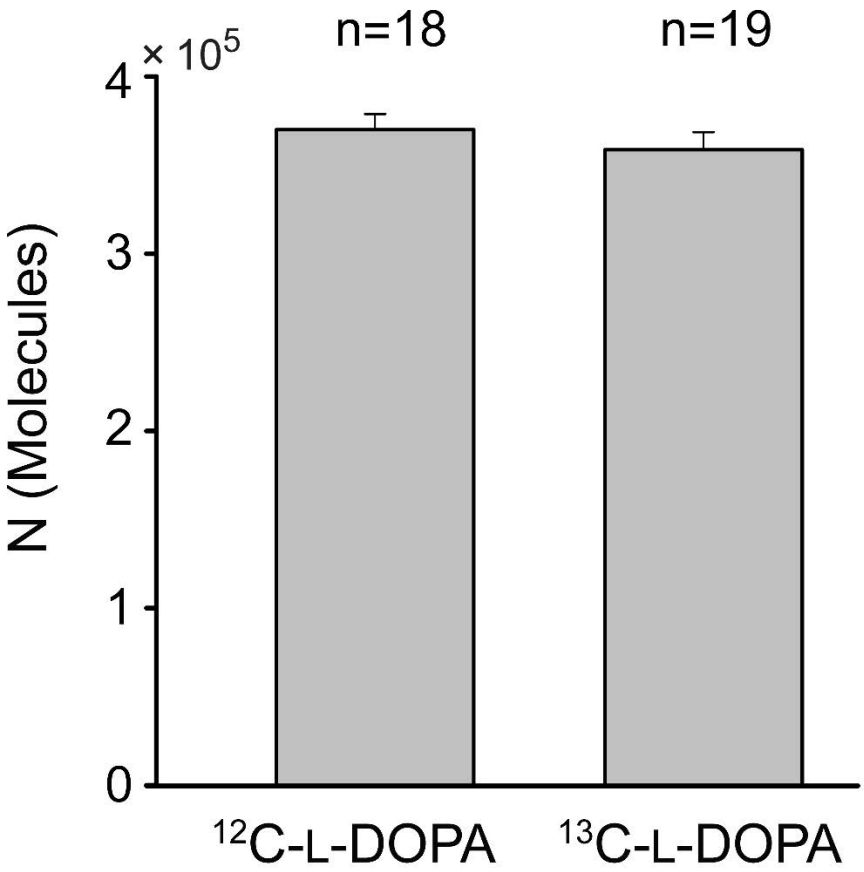

Figure S2. Investigation of the impact of isotopically labeled L-DOPA on dopamine release from cells. Comparison of number of molecules released during exocytosis when PC12 cells were treated with ^{12}C-L-DOPA and ^{13}C-L-DOPA. Error bars are SEM; n-number of cells tested.

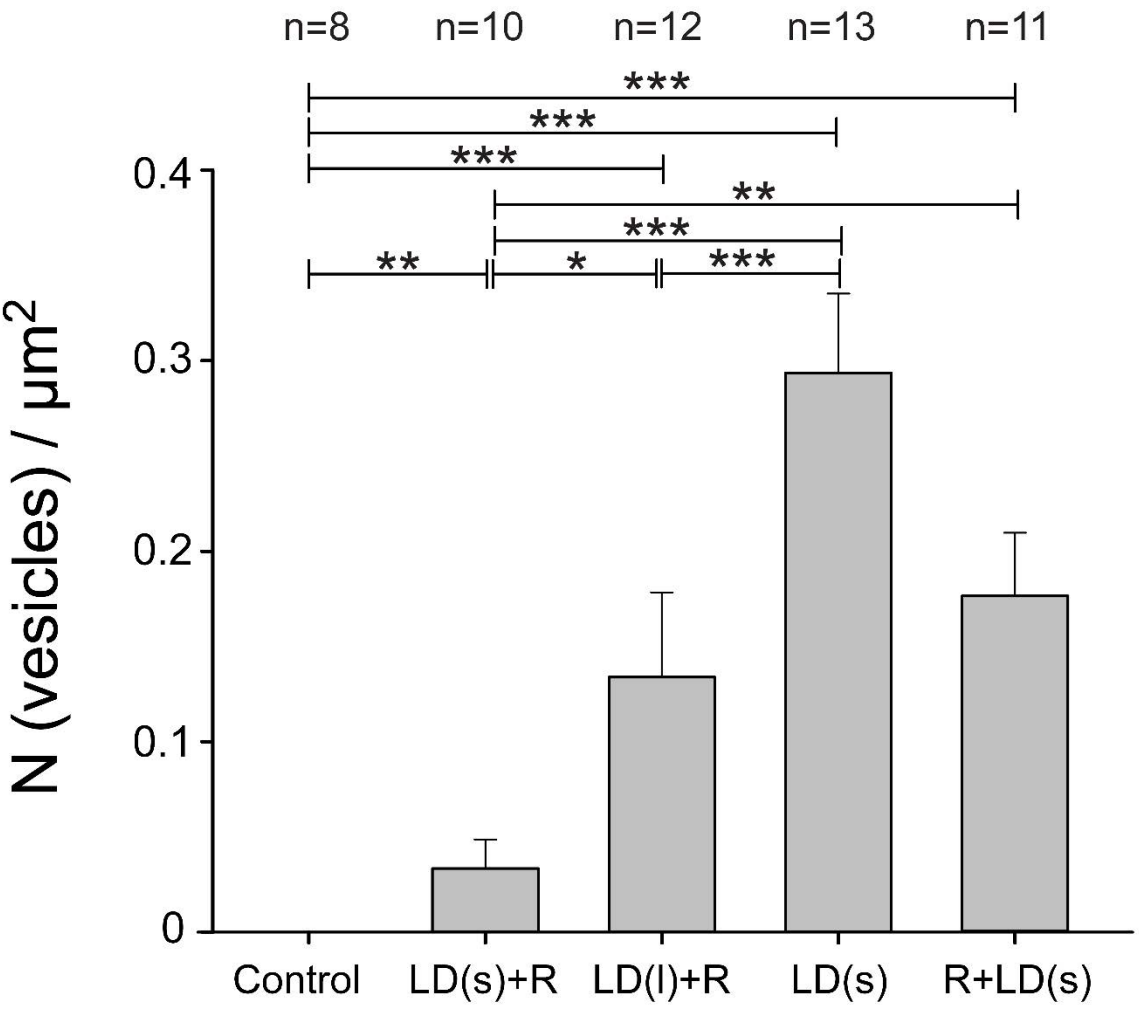

Figure S3. Vesicle density for treated samples. Error bars are SEM, One-way ANOVA on ranks: *p< 0.05, **p<0.01 and ***p<0.001; n-number of cells tested. Abbreviations: LD(s) - 1.5 h L-DOPA, short exposure; LD(l) - 12 h L-DOPA, long exposure; R - reserpine, 1-h exposure.

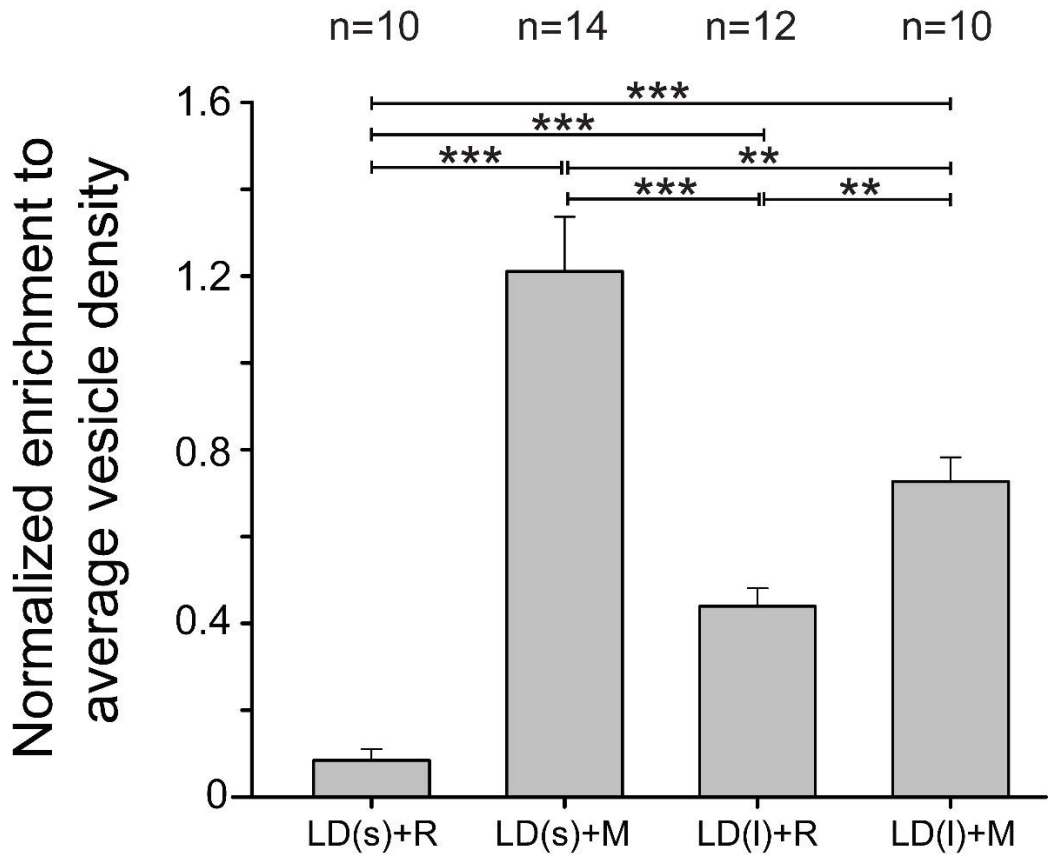

Figure S4. NanoSIMS enrichment data for control experiments of reserpine impact to vesicle leakage. ^{13}C-enrichment normalized to average vesicle density from each group of samples. Error bars are SEM, One-way ANOVA on ranks: **p<0.01 and ***p<0.001; n - number of cells tested. Abbreviations: LD(s) - 1.5 h L-DOPA, short exposure; LD(l) - 12 h L-DOPA, long exposure; R – reserpine, 1-h exposure; M - cell media, 1-h exposure.

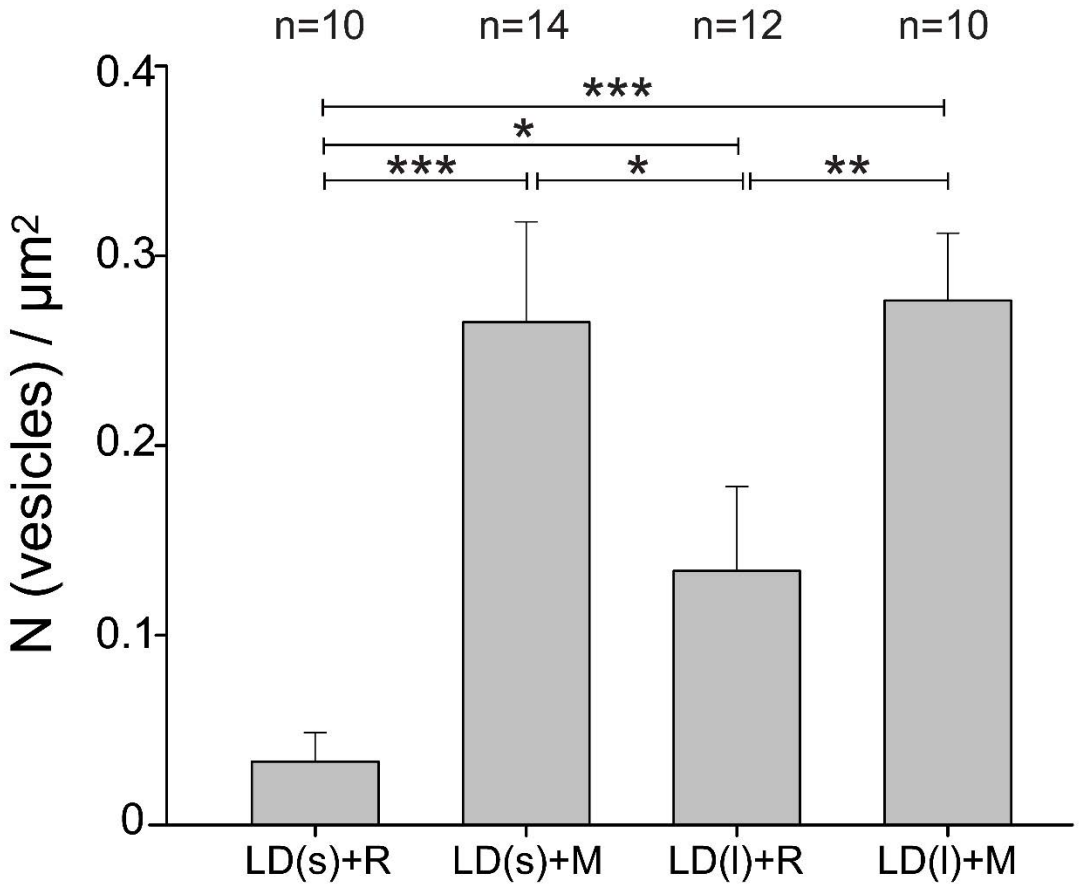

Figure S5. Vesicle density for samples treated with cell media compared to L-DOPA-reserpine treatments. Error bars are SEM, One-way ANOVA on ranks: *p< 0.05, **p<0.01 and ***p<0.001, n-number of cells tested. Abbreviations: LD(s) - 1.5 h L-DOPA, short exposure; LD(l) - 12 h L-DOPA, long exposure; R – reserpine, 1-h exposure; M - cell media, 1-h exposure.

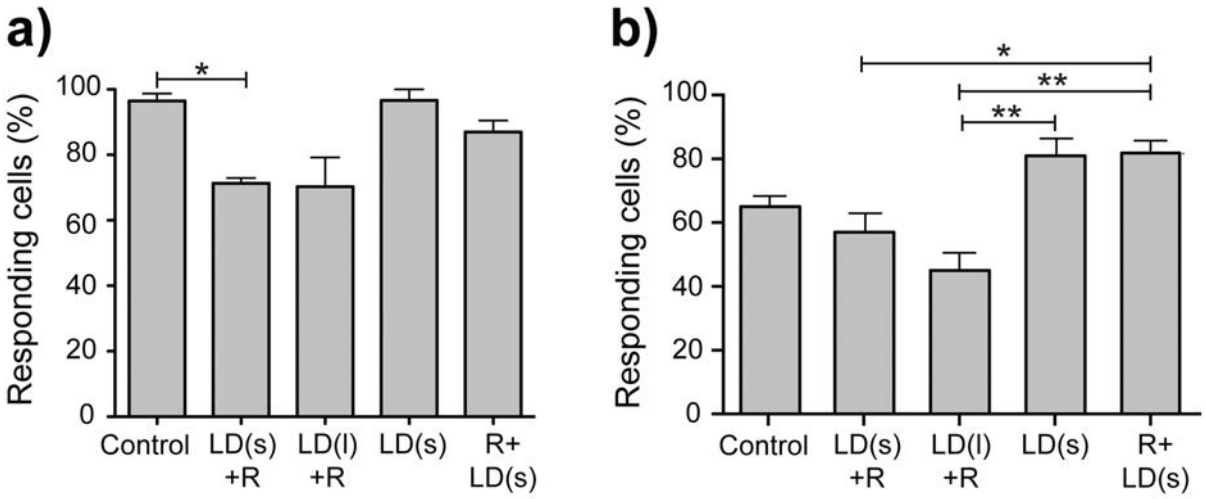

Figure S6. Cell response data for different treatments of PC12 cells obtained by electrochemical techniques. (a) Intracellular vesicle cytometry. (b) Single cell amperometry. Error bars are SEM, One-way ANOVA on ranks: *p< 0.05, **p<0.01. Abbreviations: LD(s) - 1.5 h L-DOPA, short exposure; LD(l) - 12 h L-DOPA, long exposure; R – reserpine, 1-h exposure.

Supporting Discussion

Verification of VMAT1 blockage by reserpine. In order to confirm that dopamine depletion with reserpine is not the result of experimental artifacts, we replaced reserpine with cell media (M) for 1 h, as a control (Figures S4 and S5). The data for both exposure times with ^{13}C- L-DOPA, 1.5 h and 12 h, shows significant difference in normalized enrichment between reserpine and media treated cells. This experiment confirms that dopamine depletion is related to VMAT1 inhibition.

Consideration of possible L-DOPA cytotoxicity 12-h exposure. One should consider that during long L-DOPA administration, the cell viability might be impacted by cytotoxicity. It has been reported that PC12 cells exposed to 100 μM L-DOPA for periods of 6 and 24 h exhibit reduction in cell number between approximately 15 and 72% due to the formation of reactive oxidative species.[S1] If the data in Figure S4, when the cells are post-treated with cell media, is compared, it is apparent that normalized enrichment for LD(L)+M is significantly lower than one with 1.5 h L-DOPA administration. One would expect opposite trend in this data set and it might be attributed to cytotoxicity of L-DOPA. Yet, while performing electrochemical experiments, we collected the data related to the cell responsivity (Figure S6). Here we could not observe any difference in cell response data between 1.5 h (LD(S)+R) and 12 h (LD(L)+R) L-DOPA exposure acquired by intracellular cytometry, whereas single cell amperometry showed lower cell response for long exposure yet not significant.

Comparison between imaging data obtained with ImageJ plugin OpenMIMS and MATLAB plugin Look@NanoSIMS. In Figure S7 we compare $^{13}C^{14}N^{-}/^{12}C^{14}N^{-}$ ratio images obtained with ImageJ plugin OpenMIMS (Figure S7a-b) with images from the MATLAB plugin Look@NanoSIMS (Figure S7c). In this work we used the HSI (hue-saturation-intensity) images as shown in Figure 2. However, even though the HSI image (Figure S7a) is similar to the ratio images (Figures. S7-c), revealing the same localization of

enriched ^{13}C-dopamine, there is a difference in that the HSI image is a combination of the ratio value and the counts of one of the masses for the intensity in order to generate pixels in the RGB color space (nrims.harvard.edu/files/nrims/files/openmims-manual.pdf). This allows the cellular morphology to be revealed (such as the cell nucleus) and the HSI image does not look as flat as the ratio images (Figure S7b-c). Thus, in this study we used the MATLAB plugin Look@NanoSIMS to generate the $^{13}C^{14}N^-/^{12}C^{14}N^-$ ratio images, that being in the same matrix, could easily be used for subsequent data analysis by the MATLAB in-house written routine.

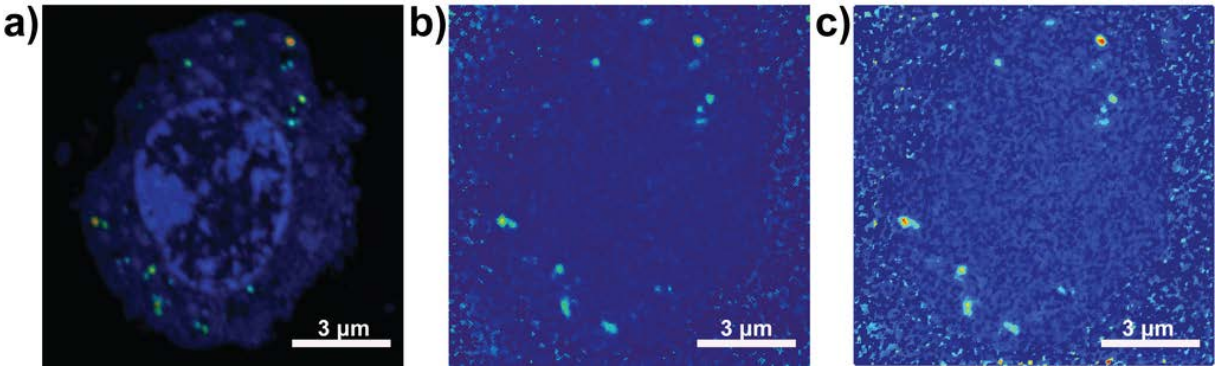

Figure S7. NanoSIMS $^{13}C^{14}N^-/^{12}C^{14}N^-$ ratio images of a PC12 cell exposed to ^{13}C-L-DOPA for 1.5 h. The ImageJ plugin OpenMIMS: (a) HSI (hue-saturation-intensity) image, median filter ratio radius of 1.5. (b) $^{13}C^{14}N^-/^{12}C^{14}N^-$ ratio image, median filter ratio radius of 1.5. **MATLAB plugin Look@NanoSIMS:** (c) $^{13}C^{14}N^-/^{12}C^{14}N^-$ ratio image, median filter: 3 by 3 pixels. All images contain 6 layers, FoV: 11×11 µm.

References

[S1] Basma, A. N.; Morris, E. J.; Nicklas, W. J.; Geller, H. M. L-DOPA Cytotoxicity to PC12 Cells in Culture is *via* its Autoxidation. *J. Neurochem.* **1995**, *64*, 825-832.